

Geometrical Dependence in Fixtures for 2D Multipole Micromagnets Magnetization Patterning

Miriam Martinez-Muñoz¹, Efren Diez-Jimenez¹, Gabriel Villalba Alumbroeros¹,
Marcin Michalowski², and Alberto Lastra-Sedano³

¹Mechanical Engineering Area, Universidad de Alcalá, Spain
gabriel.villalba@edu.uah.es, efren.diez@uah.es, miriam.martinezm@uah.es

²Warsaw University of Technology, Inst. Micromechanics & Photonics, Faculty of Mechatronics, Poland
m.michalowski@mchtr.pw.edu.pl

³Physics and Mathematics Department, Universidad de Alcalá, Spain
alberto.lastra@uah.es

Abstract — Different approaches have been used for micro-magnets multipole magnetization like fixed micro-fixtures, thermomagnetic patterning or laser machining. With previous techniques, inversion of magnetic polarizations is only partially achieved. In this work, a preliminary design of the fixtures for micro-magnets with 10, 100 and 1000 μm thickness is done. The magnetizing field dependence in respect to the geometrical parameter of the fixture is analyzed. Maps of the required current permit to pre-select an adequate pulse power source. An experimental test has been done in order to validate designs. Design recommendations to optimize the magnetizing field and to minimize the current, thus the heat, are given.

Index Terms — Magnetic polarization patterning, magnetizing fixtures, micro-magnets.

I. INTRODUCTION

Electromechanical systems miniaturization of has become one of the pillars for microelectronics development. Motors [1]–[4], clutches/brakes [5]–[8], micro-magnetic gears [9], [10], vibrational energy harvesters/dampers [11] and other micro-electromagnetic devices [12] have inspired growing interest in recent years.

Up to now, if micro-magnetic assemblies are required, the most common approach is to machine small magnets out of larger bulks and then axially magnetize the individual micro-magnets and subsequently assembly them into the micro-system. This is a cost-intensive manufacturing process because magnets are mostly magnetized before assembly and handling and positioning such micro-magnets is not straightforward. Post-assembly magnetizations are also possible [13],[14]. Alternatively, multipole magnetization of assembled micro-magnets

may provide a solution to previous technical problems.

In general, multi-pole magnetic structures can be created by pulse magnetization [15]. A magnetizing fixture with copper wire is used. If a high pulse current passes through the fixture, it produces a magnetizing field strong enough to permanently magnetize the micro-magnet. Special considerations have to be taken when operating at low temperatures because materials magnetic properties may vary significantly [16], [17]. Pulsed magnetization is a macroscale standard process [18]. However, for micro-magnets, this cannot be easily done because fixture has to be smaller than micro-magnets themselves, complicating the whole process [19].

Different approaches have been used for micro-magnets multipole magnetization. Previous developments have demonstrated the creation of multipole in hard magnetic films [20] using a combination of fixed electrical conductors and soft magnetizing heads to imprint smm period of magnetic north/south poles.

Moreover, thermomagnetic patterning has been also used to make patterns with lateral dimensions down to ~ 70 μm but only in the relative surface of the layer (1- μm deep) [21]. Additionally, a technique based on the use of a single laser-machined soft magnetic head to selectively reverse the magnetization direction in a hard magnetic layer was developed [22]. The main limitation of previous described techniques is that the inversion of the magnetic polarizations is only superficially achieved, thus the magnetic product remaining in the polarized volumes is smaller than the potential achievable one.

A radical different technique has been proposed for magnetization patterning in macroscale magnets [23]. This new technique generates magnetization patterns by magnetizing locally the magnet bulk with north or south polarization. The circular fixture is small but strong enough to magnetize a small portion of the magnet, then

the fixture is moved X-Y to a next location over the magnet and it magnetizes the next volume as desired. In this way, pixelated magnetization patterns can be created. This technique has been successfully used for macroscale magnets providing a magnetic pixel size as small as 4 mm [24] and a thicknesses larger than 3 mm.

The novelty of the present work is to use 2D multipole magnetization printing applied to micro-magnets. Such small moving magnetizing fixtures need to be carefully designed and optimized to reduce the necessary current, because the generated heat may damage the fixture. The first approach presented in this article is a trade-off analysis oriented to minimize the needed current for a certain magnetizing field level while keeping a good pixel size.

In this work, a preliminary design of the fixtures applied to micro-magnets of 10, 100 and 1000 μm thick is done. The magnetizing field dependence in respect to the geometrical parameter of the fixture is analyzed. Maps of the required current for normalized magnetizing fields are also given. These maps permit to pre-select an adequate pulse power source. An experimental test has been done in order to validate designs. Design recommendations to optimize the magnetizing field and to minimize the current, thus the heat, are given.

II. DESIGN OF FIXTURE FOR 2D MAGNETIC PATTERNING

As already stated, 2D magnetic patterning consists of one pair of movable magnetizing coils, with or without inner core, located above and below the permanent magnet bulk that locally magnetize it creating the sought pattern. This allows magnetization of shapes such as hollow cylinders or plates with alternative polarization, Fig. 1.

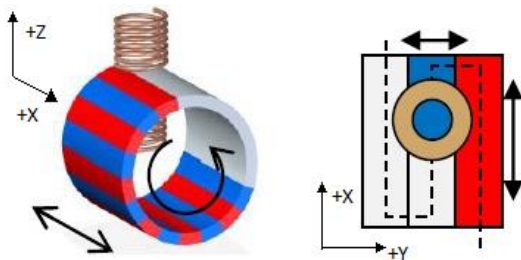


Fig. 1. 2D magnetic pattern: hollow cylinder and plate.

Figure 2 shows the diagram used for denomination of the different geometric parameters. The diagram depicts the sample to be magnetized (1), top and bottom cylindrical coils (2) and coil inner core (3). Both coils are connected in series generating the magnetizing field in the same direction. Five geometrical parameters have been defined: e – thickness of the permanent magnet bulk, R_{INT} – inner radius of the coil, R_{EXT} – outer radius

of the coil and H_C – height of the coil.

No magnetic material is considered in the inner core either, just vacuum. Although a ferromagnetic material in the inner core could increase the final magnetizing field, there are several drawbacks that prevent from its inclusion. The main pitfall is the magnetic interaction that would appear between a ferromagnetic inner core and those volumes previously magnetized. In addition, from the electrical point of view the coils inductance would be orders of magnitude larger, thus the speed of the 2D patterning would be much lower.

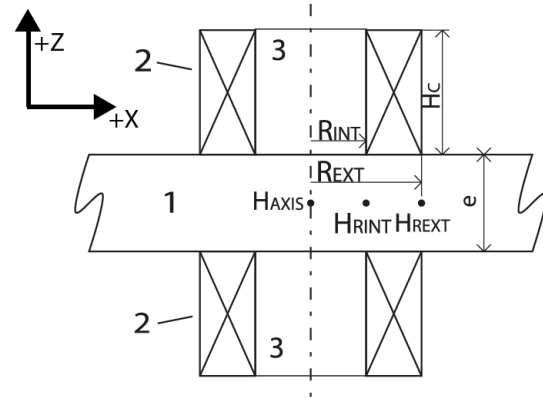


Fig. 2. Parameters of the axil-symmetrical model.

Current density perpendicular to the cross-section circulates through each coil. This current is considered uniformly distributed throughout the cross-section in all calculations. The space between coils, corresponding with the sample, will be considered as vacuum.

Magnetic field intensity generated by the designed fixtures has two symmetries: axial and middle section plane, Fig. 3 (a). It can be noticed that the lowest values are achieved in the middle section of the sample. Figure 3 (b) shows the magnetic field intensity along a radius of the middle section. This magnetic field has a maximum located at the axis and then it decreases as long as it approaches radially to the end of the coil. Just around the end of the coil, the magnetic field intensity vector is inverted to negative values. These negative values have typically an order of magnitude lower than the maximum so the effect on the adjacent magnetizations is small outside the outer radius of the coil. The variation in respect to the radius depends on the coil geometry so it is necessary to relate the shape of the applied magnetizing field for each coil geometry.

Analyzing geometrical parameters with magnetizing field cannot be practically done for any point radial points. In consequence, the magnetic field intensity (H) will be only calculated at three key points: point H_{AXIS} , located at the middle section of the sample in the symmetry axis; point H_{RINT} , located at the middle section of the sample and radially at the start of the coil and

H_{REXT} , located at the middle section of the sample and radially at the end of the coil. Magnetizing field at first point H_{AXIS} will represent the minimum magnetizing field that will be available in the axis. In a simplified manner, it is considered that if this H_{AXIS} is larger than the magnetic coercivity of the material, the sample would be 100% magnetized in the axis.

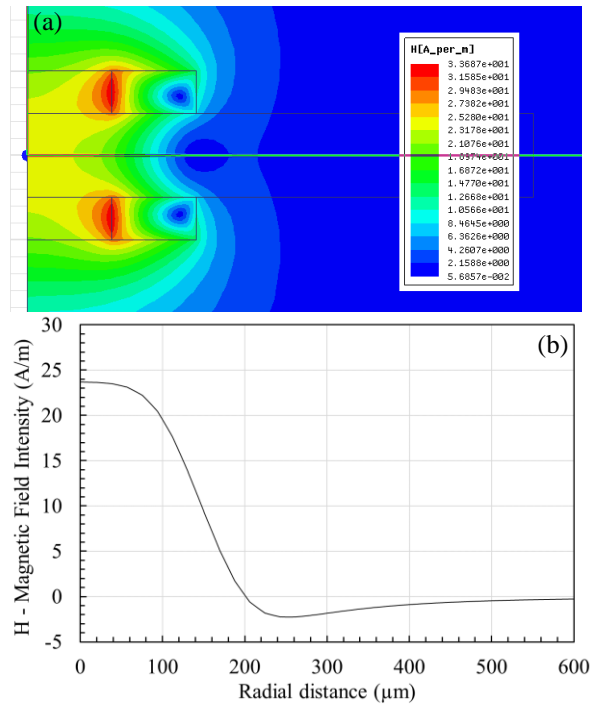


Fig. 3. (a) H - magnetic field intensity distribution ($e = 100 \mu\text{m}$, $R_{\text{INT}} = 100 \mu\text{m}$, $R_{\text{EXT}} = 200 \mu\text{m}$); (b) H - magnetic field intensity along a middle section radius.

III. FINITE ELEMENT MODEL

All calculations have been done using a finite element model (FEM) software for electromagnetic fields. The solver chosen is the magnetostatic solver. The magnetostatic field solution verifies the following two Maxwell's equations:

$$\nabla \times \vec{H} = \vec{J} \text{ and } \nabla \cdot \vec{B} = 0. \quad (1)$$

With the following relationship applicable at each material:

$$\vec{B} = \mu_0(\vec{H} + \vec{M}) = \mu_0 \cdot \mu_r \cdot \vec{H} + \mu_0 \cdot \vec{M}_p. \quad (2)$$

Where H is the magnetic field intensity, B is the magnetic field density, J is the conduction current density, M_p is the permanent magnetization, μ_0 is the vacuum permeability and μ_r is the relative permeability.

For nonlinear materials, the dependence between H and B fields is nonlinear and can be isotropic or orthotropic (in the case of anisotropic behavior, is a tensor). If nonlinearity occurs in soft materials, the software requires that BH curves for the principal

directions in the respective material(s) are provided. From these curves, energy dependence on H is extracted for each of the respective principal directions and it is used in the process of obtaining the nonlinear permeability tensor used in the Newton-Raphson iterative solution process.

There are major advantages of this formulation over other ones, including using considerably fewer computational resources (due to the scalar nature of the DOFs), not requiring gauge due to numerical stability, that significantly reduces cancellation errors and capably of automatically multiply connected iron regions [25].

The design model for the FEM is shown in Fig. 4. It is an axil-symmetrical 2D model. Z-axis is the axial symmetry axis. In this model, all the geometrical parameters from Fig. 2 can be modified automatically by software. Mesh model size is proportional to the main geometrical parameters e and R_{INT} , being finer in the surroundings interfaces.

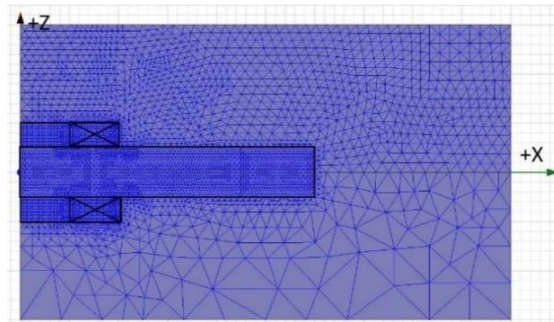


Fig. 4. Detail of the model with the initial mesh ($e = 100 \mu\text{m}$, $R_{\text{INT}} = 100 \mu\text{m}$, $R_{\text{EXT}} = 200 \mu\text{m}$, $H_c = 50 \mu\text{m}$).

Materials considered in the simulation are two: vacuum and copper. The values chosen for the properties are: magnetic permeability of vacuum $\mu_0 = 4\pi \cdot 10^{-7} \text{ H/m}$, relative permeability of copper $\mu_{\text{rCu}} = 0.99991$ and conductivity of copper at 20°C $\sigma_{\text{Cu}} = 5.8 \cdot 10^7 \text{ S/m}$.

As boundary conditions a ‘‘Balloon’’ type condition has been applied in the external edges. Balloon condition models the region out-side the model space as being nearly ‘‘infinitely’’ large. Moreover, axisymmetric condition around Z axis has been imposed.

The external excitation of the model is a constant current density uniformly distributed in the copper coil cross section, pointing perpendicular outside of the XZ plane. Value for this current density is $j=1 \text{ A/mm}^2$, allowing a result normalization since the magnetizing field depends directly on current density.

IV. SIMULATION DESCRIPTIONS AND POST-PROCESSING

Each simulation corresponds to a single combination of the four geometrical parameters described in Fig. 2.

The solver uses an adaptive meshing solver process. Typically, three to four iterations from the initial mesh have been enough for a correct convergence of the simulation. The total number of triangular elements is around 20000 elements. The mesh has been designed for achieving less than 0.03% of energy error within a simulation time of less than 5 seconds per simulation.

Table 1: List of simulations

N° sim.	e (μm)	H _C (μm)	R _{INT} (μm)	R _{EXT} (μm)
1	10	5	1.25 to 20 (1.25 step)	R _{INT} + (1.25 to 20)
2	10	1.25 to 40 (1.25 step)	2.5	3.75, 12.5 and 22.5
3	100	50	12.5 to 200 (12.5 step)	R _{INT} + (12.5 to 200)
4	100	12.5 to 400 (12.5 step)	25	37.5, 125 and 225
5	1000	500	125 to 2000 (125 step)	R _{INT} + (125 to 2000)

The simulations have been done in a workstation with an Intel Core i5-4690 with 8Gb of RAM memory.

Three different sample thicknesses have been analyzed: 10 μm, 100 μm and 1000 μm. For each, a combination of the rest of parameters has been done. Combinations are listed in Table 1.

The simulation plan has been proposed in order to assess how the coil width affects to the magnetizing field and to determine the point where increasing the coil height is not efficient anymore. Each simulation returns the magnetic field intensity in the points described in Section 2, H_{AXIS}, H_{REXT} and H_{RINT}. Some analysis can be done from the magnetic field in those three key points. For example, magnetic field at second point H_{RINT} divided by magnetic field at H_{AXIS} indicates the amount of magnetizing field at the beginning of the coil, representing the magnetized pixel width (% *Pixel*). Magnetic field at third point H_{REXT} in respect to the magnetic field at H_{AXIS} (% *Out*) indicates the type of transition between magnetized pixels. Expressions for those calculations are:

$$\% \text{ Pixel} = \frac{H_{RINT}}{H_{AXIS}} \cdot 100, \quad (3)$$

$$\% \text{ Out} = \frac{H_{REXT}}{H_{AXIS}} \cdot 100. \quad (4)$$

Furthermore, voltages can be calculated as:

$$V = I \cdot R = j \cdot S \cdot \rho \cdot \frac{l}{S} = j \cdot \rho \cdot \pi \cdot (R_{INT} + R_{EXT}). \quad (5)$$

Where I is the total current circulating across the fixture cross-section, R is the total resistance of the cylindrical coil considered as a complete cylinder; j is the current density, as default 1 A/mm²; $S = H_C \cdot (R_{EXT} - R_{INT})$ is the cross-section surface; l is the length, in this

case considered as $l = 2\pi \cdot (R_{INT} + \frac{R_{EXT} - R_{INT}}{2})$; and ρ is the copper resistivity. Copper resistivity value is critical for the right determination of voltage. However, as the cylinder will heat up by joule effect, the resistivity property varies with time. Indeed, the maximum admissible current, thus the maximum magnetizing field, will depend on this temperature rise. As a first approximation, the chosen value is the one considering operation at intermediate temperature between 20°C and copper fusion temperature which is 1085 °C. Therefore, $\rho = \rho_{20} \cdot (1 + \alpha \cdot \Delta T) = 1.71 \cdot 10^{-8} (1 + 3.9 \cdot 10^{-3} \cdot (545 - 20)) = 5.13 \cdot 10^{-8} \Omega m$.

In this calculation, skin effect has been considered negligible. This assumption is fairly valid provided that pulse duration is longer than 10 ms for copper conductors [26].

In terms of thermal behavior, the power density generated by the coil can be expressed as:

$$P_{Vol} = \frac{I^2 \cdot R}{H_C \cdot \pi \cdot (R_{EXT}^2 - R_{INT}^2)} = \frac{(j \cdot S)^2 \cdot \rho \cdot \frac{l}{S}}{H_C \cdot \pi \cdot (R_{EXT}^2 - R_{INT}^2)} = \frac{j^2 \cdot S \cdot \rho \cdot l}{H_C \cdot \pi \cdot (R_{EXT}^2 - R_{INT}^2)} = \frac{j^2 \cdot \rho \cdot H_C \cdot (R_{EXT} - R_{INT}) \cdot 2\pi \cdot (R_{INT} + \frac{R_{EXT} - R_{INT}}{2})}{H_C \cdot \pi \cdot (R_{EXT}^2 - R_{INT}^2)} = j^2 \cdot \rho. \quad (6)$$

It implies that power density, and thus volumetric temperature raise, is independent of coil geometry. But, as current density needs to be large for achieving a magnetizing field, geometries with lower magnetizing field capacity would suffer a higher temperature.

V. RESULTS AND DISCUSSION

A. Thickness e = 10 μm - Simulation number 1 and 2

Next Figs. 5-7 present the results from simulation number 1. In this simulation, the magnetizing field has been analyzed by varying R_{INT} and R_{EXT} for a single height of the coil value H_C = 5 μm.

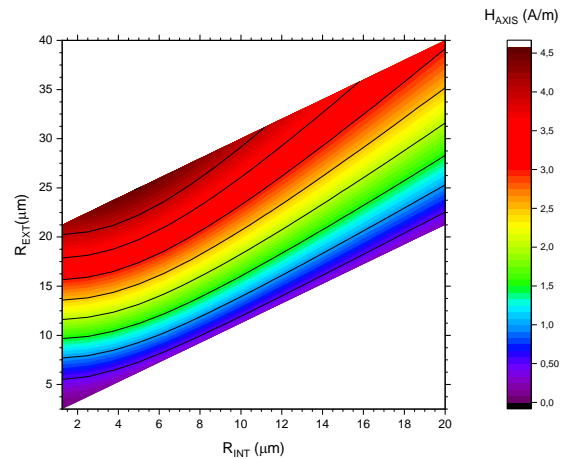


Fig. 5. H_{AXIS} in respect to R_{INT} and R_{EXT} for e = 10 μm and H_C = 5 μm.

Figure 5 shows magnetizing field contour map H_{AXIS} for different combinations of R_{INT} and R_{EXT} , with a thickness e and a fixed coil height H_C . The values vary from 0.12 to 4.52 A/m for a current density of 1 A/mm². The maximum values are achieved at $R_{INT} = 5 \mu\text{m}$ and $R_{EXT} = 25 \mu\text{m}$. The minimum values are achieved at $R_{INT} = 1.25 \mu\text{m}$ and $R_{EXT} = 2.5 \mu\text{m}$. For any R_{INT} value, magnetizing field increases when increasing R_{EXT} , i.e., the thicker is the coil, the larger the magnetizing field is. H_{AXIS} behavior is almost linear with respect to R_{INT} and R_{EXT} . This means that it can be worth in terms of magnetizing field to use thick coils. However, by using thicker coils the pixel will also be larger, decreasing the pattern resolution.

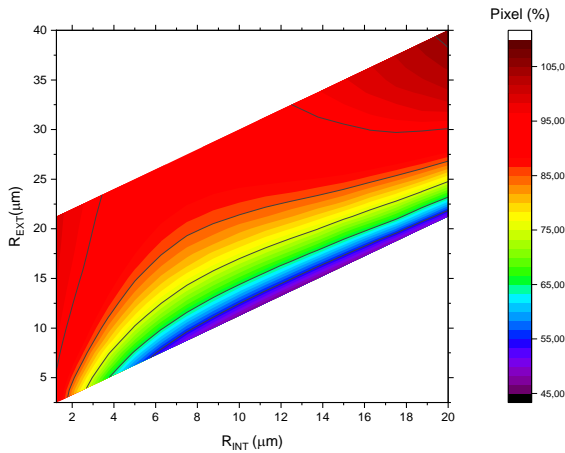


Fig. 6. % Pixel in respect to R_{INT} and R_{EXT} for $e = 10 \mu\text{m}$ and $H_C = 5 \mu\text{m}$.

Figure 6 presents a contour map of % Pixel for different combinations of R_{INT} and R_{EXT} , with a thickness e and a fixed coil height H_C . The values vary from 46.8% to 106.2%. The maximum values are achieved at $R_{INT} = 20 \mu\text{m}$ and $R_{EXT} = 40 \mu\text{m}$. In this case, the magnetizing field in the coils proximities is even larger than in the axis because the pixel diameter, given by R_{INT} , is very large. The minimum values are achieved at $R_{INT} = 10 \mu\text{m}$ and $R_{EXT} = 13.75 \mu\text{m}$. This case has a sharp decrease from axis to coil beginning. There is a wide number of combinations where % Pixel remains between 85-95%.

Combining Fig. 5 and Fig. 6, we can determine that a combination around $R_{INT} = 12.5 \mu\text{m}$ and $R_{EXT} = 25 \mu\text{m}$ is a good trade-off between high magnetizing field, high % Pixel and pixel diameter without excessive coil thickness.

Figure 7 displays a contour map of the % Out for different combinations of R_{INT} and R_{EXT} , with a thickness e and a fixed coil height H_C . The values vary from 0% to 53%. The maximum values are achieved at $R_{INT} = 1.25 \mu\text{m}$ and $R_{EXT} = 2.5 \mu\text{m}$. In this case, the magnetizing field outside the coil is very large for an adequate pixel

resolution, significantly affecting to adjacent volumes. Minimum values are achieved at $R_{INT} = 1.5 \mu\text{m}$ and $R_{EXT} = 20 \mu\text{m}$. This combination has a negligible effect on the adjacent volumes. Again, there is a vast number of combinations where % Out remains between 0-10%.

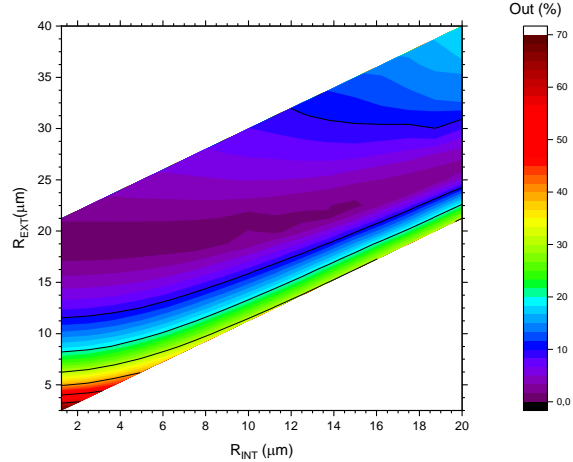


Fig. 7. % Out in respect to R_{INT} and R_{EXT} for $e = 10 \mu\text{m}$ and $H_C = 5 \mu\text{m}$.

For the pre-selected combination of $R_{INT} = 12.5 \mu\text{m}$ and $R_{EXT} = 25 \mu\text{m}$, the % Out is 5% which reinforces the benefits of this combination selection.

Next Figs. 8-9 show the results from simulation number 2. In this simulation, the magnetizing field has been analyzed by varying the height of the coil H_C , for three specific combinations of R_{INT} and R_{EXT} ($R_{INT} = 2.5 \mu\text{m}$ combined with $R_{EXT} = 3.75, 12.5$ and $22.5 \mu\text{m}$).

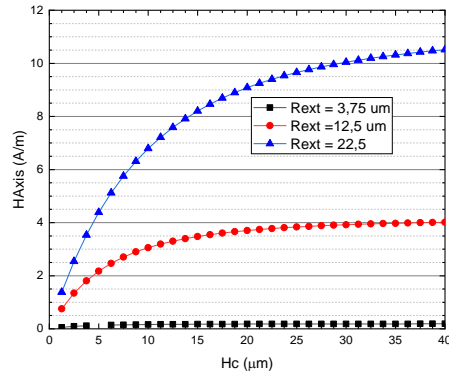


Fig. 8. H_{AXIS} in respect to H_C for $e = 10 \mu\text{m}$, $R_{INT} = 2.5 \mu\text{m}$ combined with $R_{EXT} = 3.75, 12.5$ and $22.5 \mu\text{m}$.

Figure 8 displays three plots of the magnetizing field H_{AXIS} as a function of coil height H_C with R_{INT} and e fixed, and for different coils width given by $R_{EXT} - R_{INT}$. It can be observed that all the plots have an asymptotic behavior. This means that for a certain coil value of coil height it will not be worth to continue increasing H_C .

Increasing H_C will also raise the total resistance and therefore the voltage needed for a certain current

It has been selected $\frac{3}{4}$ of maximum magnetizing field as the optimal point for coil height. For the cases of $R_{EXT} = 12.5$ and $22.5 \mu\text{m}$ the coil height corresponding with $\frac{3}{4}$ of maximum magnetizing is $H_C \approx (R_{EXT} - R_{INT})$. In the case of $R_{EXT} = 3.75 \mu\text{m}$, the ratio $H_C/(R_{EXT} - R_{INT}) = 0.85$, slightly lower than for larger coil width. Therefore, a design guideline for coil height is to choose a similar height than coil thickness.

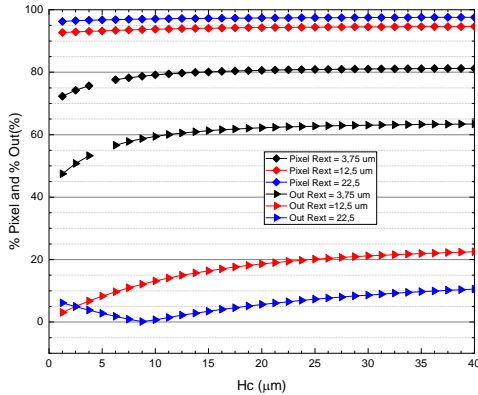


Fig. 9. % Pixel and % Out in respect to H_C for $e = 10 \mu\text{m}$, $R_{INT} = 2.5 \mu\text{m}$ with $R_{EXT} = 3.75, 12.5$ and $22.5 \mu\text{m}$.

Figure 9 shows three plots of % Pixel and % Out as a coil height H_C function with R_{INT} and e fixed, and for different coils width given by $R_{EXT} - R_{INT}$. Regarding % Pixel, asymptotic value is quickly achieved. No significant variation from the initial value and the asymptotic one is found. Therefore, coil height does not affect to % Pixel. On the contrary, % Out varies from initial values to asymptotic ones. This variation can be more than 10% of the absolute value of % Out. Thus, values of % Out from Fig. 8, where H_C was just $5 \mu\text{m}$, should be corrected for the case of larger height coils.

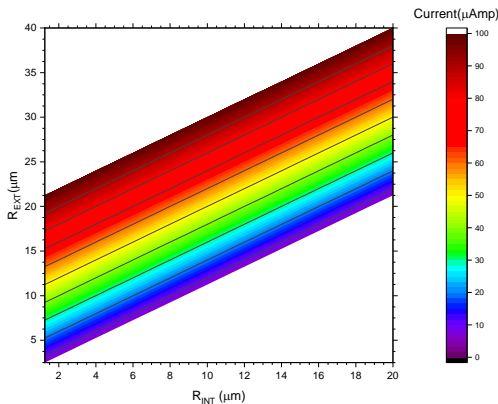


Fig. 10. Currents in respect to R_{INT} and R_{EXT} for $e = 10 \mu\text{m}$ and $H_C = 5 \mu\text{m}$.

Current depends directly on current density and on the cross section. Hence, total current flowing through a cross section is directly proportional to $(R_{EXT} - R_{INT})$, i.e., coil width. This behavior is described in Fig. 10. Minimum values for total current are found in those combinations with thinner section while maximums are for the thicker ones. The order of magnitude in Fig. 10 is micro-ampere. This figure can be used to determine the current to be provided by the pulse power source.

B. Thickness $e = 100 \mu\text{m}$ - Simulation n° 3 and 4

Next Fig. 11 shows the results from simulation number 3. In this simulation, the magnetizing field has been analyzed by combining R_{INT} and R_{EXT} for a single height of the coil value $H_C = 50 \mu\text{m}$.

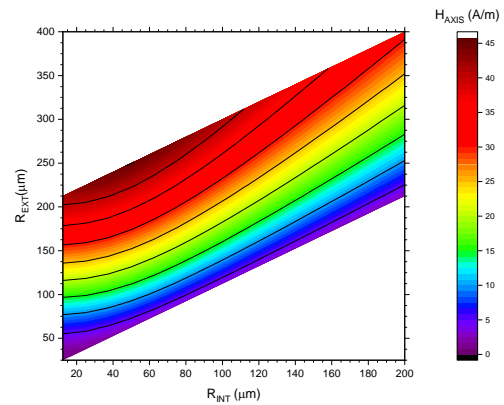


Fig. 11. H_{AXIS} in respect to R_{INT} and R_{EXT} for $e = 100 \mu\text{m}$ and $H_C = 50 \mu\text{m}$.

Figure 11 presents a magnetizing field H_{AXIS} contour map for different combinations of R_{INT} and R_{EXT} , with a thickness e and a fixed coil height H_C . Values vary from 1.2 to 45.2 A/m for a current density of 1 A/mm², ten times larger than for $e = 10 \mu\text{m}$. Maximum values are achieved at $R_{INT} = 50 \mu\text{m}$ and $R_{EXT} = 250 \mu\text{m}$. Minimum values are achieved at $R_{INT} = 12.5 \mu\text{m}$ and $R_{EXT} = 25 \mu\text{m}$. This result is almost the same presented in Fig. 5 but one order of magnitude larger in the magnetizing field and in geometrical values. It makes sense since all the geometrical parameters have been scaled one order of magnitude so volume does. % Pixel and % Out for simulation 3 results are also similar to those presented in Figs. 6-7 and so do conclusions.

Next Figs. 12-13 show the results from simulation number 4. In this simulation, magnetizing field has been analyzed by varying the coil height H_C , with three specific combinations of R_{INT} and R_{EXT} ($R_{INT} = 25 \mu\text{m}$ combined with $R_{EXT} = 375, 125$ and $225 \mu\text{m}$).

Figure 12 presents three plots of the magnetizing field H_{AXIS} as a function of coil height H_C with R_{INT} and fixed e , and for different coils width given by $R_{EXT} - R_{INT}$. It can be observed that all the plots have

an asymptotic behavior. It means that for a certain coil height value, it will not be worth to continue increasing H_C . Increasing H_C will also raise the total resistance and therefore the voltage needed for a certain current.

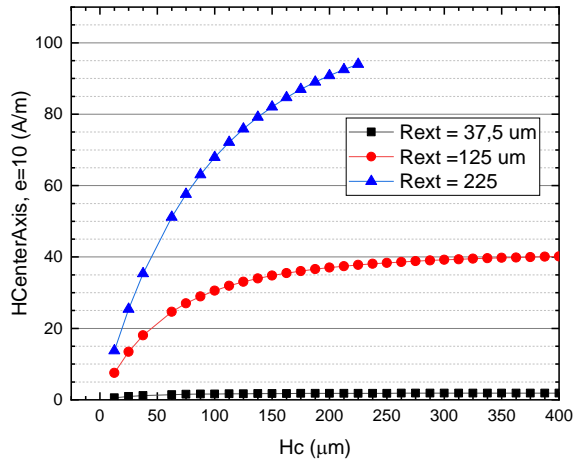


Fig. 12. H_{AXIS} in respect to H_C for $e = 100 \mu\text{m}$, $R_{INT} = 25 \mu\text{m}$ combined with $R_{EXT} = 375, 125$ and $225 \mu\text{m}$.

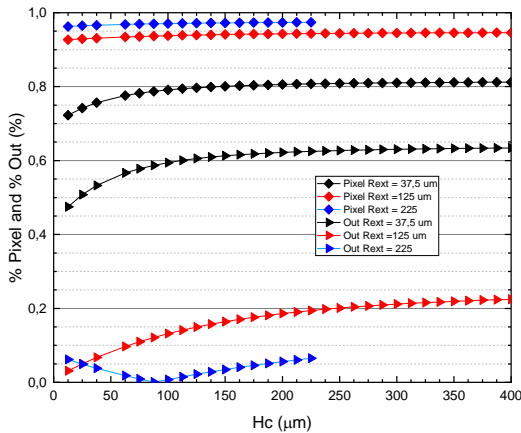


Fig. 13. % Pixel and % Out in respect to H_C for $e = 100 \mu\text{m}$, $R_{INT} = 25 \mu\text{m}$ with $R_{EXT} = 375, 125$ and $225 \mu\text{m}$.

Figure 13 gathers three plots of % Pixel and % Out as a function of coil height H_C with R_{INT} and fixed e , and for different coils width given by $R_{EXT} - R_{INT}$. Regarding % Pixel the asymptotic value is quickly achieved. No significant variation from the initial value and the asymptotic one is found. Therefore, coil height does not affect to % Pixel. On the contrary, % Out varies from initial values to asymptotic ones. This variation can be more than the 10% of the absolute value of % Out. Thus, % Out values from figure 13, where H_C was just $50 \mu\text{m}$, should be corrected in larger height coils cases.

The behavior described in Fig. 10 is the same than described in Fig. 14 but currents are two order of

magnitude larger according to its dependence on cross-section size.

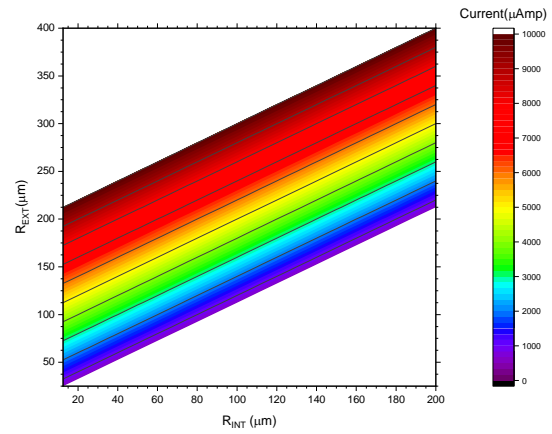


Fig. 14. Currents in respect to R_{INT} and R_{EXT} for $e = 100 \mu\text{m}$ and $H_C = 50 \mu\text{m}$.

C. Thickness $e = 1000 \mu\text{m}$ - Simulation number 5

Next Fig. 15 displays the results from simulation number 5. In this simulation, the magnetizing field has been analyzed by combining R_{INT} and R_{EXT} for a single height of the coil value $H_C = 500 \mu\text{m}$.

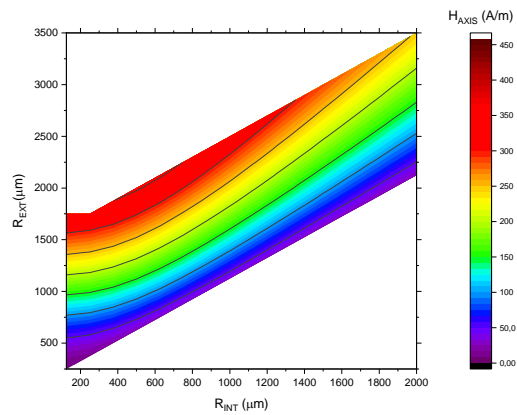


Fig. 15. H_{AXIS} in respect to R_{INT} and R_{EXT} for $e = 1000 \mu\text{m}$ and $H_C = 500 \mu\text{m}$.

Figure 15 presents a magnetizing field H_{AXIS} contour map for different combinations of R_{INT} and R_{EXT} , with a thickness e and a fixed coil height H_C . Values vary from 12 to 452 A/m with a current density of 1 A/mm^2 . The maximum values are achieved at $R_{INT} = 500 \mu\text{m}$ and $R_{EXT} = 200 \mu\text{m}$. The minimum values are achieved at $R_{INT} = 125 \mu\text{m}$ and $R_{EXT} = 250 \mu\text{m}$. For any R_{INT} value, magnetizing field increases when increasing R_{EXT} , i.e., the thicker is the coil, the larger the magnetizing field is. This result is almost the same presented in Fig. 5 but two orders of magnitude larger in the magnetizing fields

and in the geometrical values. The rest of the results for simulation 5 corresponding to previous Figs. 6-7 are also similar and so conclusions. In any case, the results are presented in next Figs. 16-17.

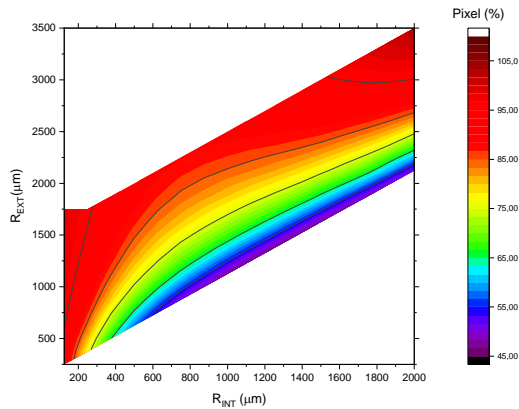


Fig. 16. % Pixel in respect to R_{INT} and R_{EXT} for $e = 1000 \mu\text{m}$ and $H_c = 500 \mu\text{m}$.

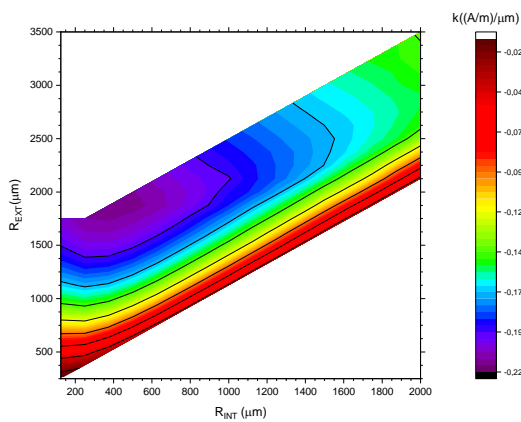


Fig. 17. % Out in respect to R_{INT} and R_{EXT} for $e = 1000 \mu\text{m}$ and $H_c = 500 \mu\text{m}$.

Combining Fig. 16 and Fig. 17, we can determine that a combination around $R_{INT} = 1250 \mu\text{m}$ and $R_{EXT} = 2000 \mu\text{m}$ is a good trade-off between high magnetizing field, high % Pixel and pixel diameter without excessive coil thickness. For the pre-selected combination of $R_{INT} = 1250 \mu\text{m}$ and $R_{EXT} = 2500 \mu\text{m}$, the % Out is 5% which reinforces the trade-off benefits of this combination.

Figure 18 presents currents calculations from simulation number 5. The behavior described in Fig. 18 is the same than described in Fig. 20 but currents are two orders of larger according to its dependence on cross-section size.

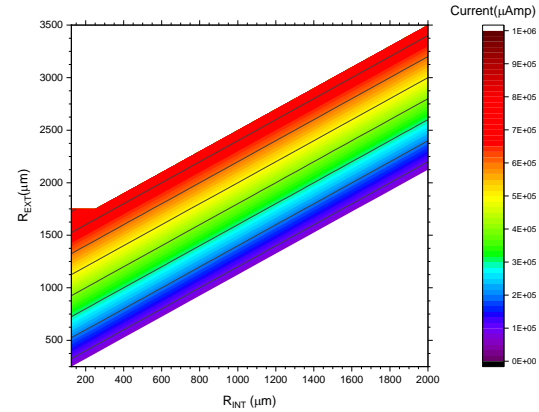


Fig. 18. Currents in respect to R_{INT} and R_{EXT} for $e = 1000 \mu\text{m}$ and $H_c = 500 \mu\text{m}$.

D. Coil design model – Experimental validation

An experimental validation of the models has been done by using two real millimetric size coils. As coils two air core fixed micro-inductors from electronics components provider have been mounted on a 3D printed frame as shown in Fig. 19. More specifically, coils are two units of model AL12A18N5GTR from AVX RF Inductors corp. with dimensions are: $R_{INT} = 1000 \mu\text{m}$, $R_{EXT} = 1500 \mu\text{m}$ and $H_c = 5800 \mu\text{m}$. Coils are made by a 0.5 mm diameter wire wrapped around with 5 wire turns. Separation distance of coils was set for $e = 1000 \mu\text{m}$.

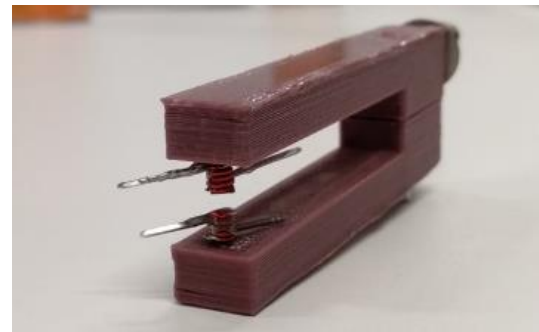


Fig. 19. Prototype for model validation: two units of model AL12A18N5GTR separated $e = 1000 \mu\text{m}$.

Coils have been connected in serial to an external power source and mounted on a XY displacement table as shown in Fig. 20. The magnetic field generated by the coils has been measured in the middle of the coils separation empty space, located in the axis. In order to measure the magnetic field, a GM08 model magnetometer from Hirst Magnetic Instruments Ltd with transvers hall

probe has been used.

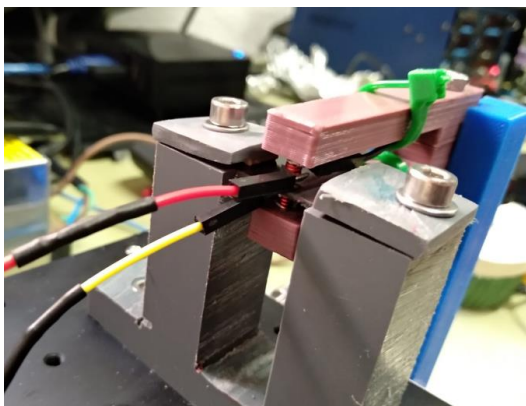


Fig. 20. Prototype coils connected in series and mounted on the XY displacement table.

The current applied has been 1.01 across a total section of 0.98 mm^2 , i.e., an approximate current density of 1 A/mm^2 . With this current density applied, the magnetic field obtained has been 325 A/m .

From Fig. 15 and with the combination of $R_{\text{INT}} = 1000 \text{ }\mu\text{m}$, $R_{\text{EXT}} = 1500 \text{ }\mu\text{m}$, the value of the expected magnetic field at H_{AXIS} is 175 A/m . It is important to notice that this value is expected if the coil height was $500 \text{ }\mu\text{m}$. However, for the experimental case, coil height was ten times larger which means that values should be in the asymptotic point. Analyzing Figs. 8 and 12, ($R_{\text{INT}} = 12.5 \text{ }\mu\text{m}$ and $125 \text{ }\mu\text{m}$ respectively) values at the asymptotic point are almost twice the value for $H_{\text{C}} = 5$ and $50 \text{ }\mu\text{m}$ respectively. Therefore, the expected H_{AXIS} value has to be corrected by a factor of two, reaching 350 A/m , which is in good agreement with the measured value.

VI. CONCLUSION

This work presents the potential of 2D multipole magnetization printing applied to micro-magnets is as a technique for microsystems magnets. The research shown in this article is a trade-off analysis to minimize the needed current, and thus voltage, for a certain magnetizing field level while keeping a good pixel size.

In this work, the technique is oriented to micro-magnets with 10 , 100 and $1000 \text{ }\mu\text{m}$ thickness. The magnetizing field dependence in respect to the fixtures geometrical parameter is analyzed. Some design recommendations are:

- The thicker is the coil, the larger the magnetizing field is. However, by using thicker coils the pixel will also be larger, decreasing the pattern resolution.
- There is a vast number of geometrical combinations where % Pixel remains between 85-95%.
- There is a vast number of combinations where %

Out remains between 0-10%.

- An optimal coil height selection is to choose a height similar to the coil thickness.
- The geometrical dependence is the same for the three orders of magnitude analyzed.
- Current flowing through a cross section is directly proportional to coil width.
- Volumetric Joule effect heat is independent of the geometry of the coil.

Maps of the required current for normalized magnetizing fields are also given. These maps permit to pre-select an adequate pulse power source.

An experimental test has been done in order to validate simulation models with a good agreement.

Therefore, the results and conclusions presented in this work will allow to accelerate significantly trade-off procedures when designing 2D multipole magnetization patterning fixtures for specific industry applications.

ACKNOWLEDGMENT

This work has been funded by Universidad de Alcalá, under Grant No. CCGP2017-EXP/011. Authors want to recognize the work of Alba Martínez Pérez in figures preparation and English corrections.

REFERENCES

- [1] E. Diez-Jimenez, J. L. Perez-Diaz, and J. C. Garcia-Prada, "Local model for magnet-superconductor mechanical interaction: Experimental verification," *J. Appl. Phys.*, vol. 109, no. 6, pp. 063901-063901-5, 2011.
- [2] E. Diez-Jimenez, "Design and analysis of a non-hysteretic passive magnetic linear bearing for cryogenic environments," *Proc. Inst. Mech. Eng. Part J J. Eng. Tribol.*, 2014.
- [3] S. Wu, S. Zuo, X. Wu, F. Lin, and J. Shen, "Magnet modification to reduce pulsating torque for axial flux permanent magnet synchronous machines," *Appl. Comput. Electromagn. Soc. J.*, vol. 31, no. 3, pp. 294-303, 2016.
- [4] B. Rezaeealam and F. Rezaee-Alam, "Optimization of permanent magnet synchronous motors using conformal mappings," *Appl. Comput. Electromagn. Soc. J.*, vol. 32, no. 10, pp. 915-923, 2017.
- [5] R. Rizzo, A. Musolino, F. Bucchini, P. Forte, and F. Frendo, "A multi-gap magnetorheological clutch with permanent magnet," *Smart Mater. Struct.*, vol. 24, no. 7, 2015.
- [6] R. Rizzo, "An innovative multi-gap clutch based on magneto-rheological fluids and electrodynamic effects: Magnetic design and experimental characterization," *Smart Mater. Struct.*, vol. 26, no. 1, 2017.
- [7] R. Rizzo, A. Musolino, and H. C. Lai, "An electrodynamic/magnetorheological clutch powered by permanent magnets," *IEEE Trans. Magn.*, vol.

- 53, no. 2, pp. 1-7, Feb. 2017.
- [8] E. Diez-Jimenez, A. Musolino, M. Raugi, R. Rizzo, and L. Sani, "A magneto-rheological brake excited by permanent magnets," *Appl. Comput. Electromagn. Soc. J.*, vol. 34, no. 1, pp. 186-191, 2019.
- [9] M. Muñoz-Martínez, E. Diez-Jimenez, M. J. Gómez-García, R. Rizzo, and A. Musolino, "Torque and bearing reaction forces simulation of micro-magnetic gears," *Appl. Comput. Electromagn. Soc. J.*, vol. 3, 2019.
- [10] E. Diez-Jimenez, R. Sanchez-Montero, and M. Martinez-Muñoz, "Towards miniaturization of magnetic gears: Torque performance assessment," *Micromachines*, vol. 9, no. 1, p. 16, Dec. 2017.
- [11] J. L. Perez-Diaz, *et al.*, "A novel high temperature eddy current damper with enhanced performance by means of impedance matching," *Smart Mater. Struct.*, vol. 28, no. 2, p. 025034, 2019.
- [12] S. Barmada, A. Musolino, and R. Rizzo, "Equivalent network approach for the simulation of MEMS devices," *Appl. Comput. Electromagn. Soc. J.*, vol. 21, no. 1, pp. 16-25, 2006.
- [13] M.-F. Hsieh, Y.-M. Lien, and D. G. Dorrell, "Post-assembly magnetization of rare-earth fractional-slot surface permanent-magnet machines using a two-shot method," *IEEE Trans. Ind. Appl.*, vol. 47, no. 6, pp. 2478-2486, Nov. 2011.
- [14] E. Diez-Jimenez, A. Musolino, R. Rizzo, and E. Tripodi, "Analysis of the static and dynamic behavior of a non hysteretic superconductive passive magnetic linear bearing by using an electromagnetic integral formulation," *Prog. Electromagn. Res. M*, vol. 50, pp. 183-193, 2016.
- [15] Y. N. Zhilichev, "Precise multipole magnetization of disc magnet for sensor application," *IEEE Trans. Magn.*, vol. 39, no. 5, pp. 3301-3303, Sep. 2003.
- [16] E. Diez-Jimenez, *et al.*, "Magnetic and morphological characterization of Nd₂Fe₁₄B magnets with different quality grades at low temperature 5–300 K," *J. Magn. Magn. Mater.*, vol. 451, pp. 549-553, Apr. 2018.
- [17] E. Diez-Jimenez, J. L. Perez-Diaz, F. Canepa, and C. Ferdeghini, "Invariance of the magnetization axis under spin reorientation transitions in polycrystalline magnets of Nd₂Fe₁₄B," *J. Appl. Phys.*, vol. 112, no. 6, p. 063918, 2012.
- [18] J. Töpfer, B. Pawlowski, H. Beer, K. Plötner, P. Hofmann, and J. Herrfurth, "Multi-pole magnetization of NdFeB magnets for magnetic micro-actuators and its characterization with a magnetic field mapping device," *J. Magn. Magn. Mater.*, vol. 270, no. 1-2, pp. 124-129, 2004.
- [19] J. Töpfer and V. Christopher, "Multi-pole magnetization of NdFeB sintered magnets and thick films for magnetic micro-actuators," *Sensors Actuators, A Phys.*, vol. 113, no. 2, pp. 257-263, 2004.
- [20] A. Garraud, *et al.*, "Microscale magnetic patterning of hard magnetic films using microfabricated magnetizing masks," *Proc. IEEE Int. Conf. Micro Electro Mech. Syst.*, pp. 520-523, 2014.
- [21] F. Dumas-Bouchiat, *et al.*, "Thermomagnetically patterned micromagnets," *Appl. Phys. Lett.*, vol. 96, no. 10, 2010.
- [22] A. Garraud, N. M. Dempsey, and D. P. Arnold, "Microscale magnetic patterning of hard magnetic films using microfabricated magnetizing masks," in *Proceedings of the IEEE International Conference on MEMS*, pp. 520-523, 2014.
- [23] L. Fullerton, "System and Method for producing Magnetic Structures," 2015.
- [24] "Catalog of Polymagnets (R)," 2018. [Online]. Available: <http://www.polymagnet.com/>
- [25] "Ansoft Ansys Maxwell v15 - Help assistant," 2018.
- [26] W. H. Hayt, *Engineering Electromagnetics*. 1989.